POLITECNICO DI TORINO
Repository ISTITUZIONALE

Experimental Identification of the Magnetic Model of Synchronous Machines

Original
Experimental Identification of the Magnetic Model of Synchronous Machines / Armando, E.G., Bojoi, I.R., Guglielmi, P., Pellegrino, G.-.M.L., Pastorelli, M.A.. - In: IEEE TRANSACTIONS ON INDUSTRY APPLICATIONS. - ISSN 0093-9994. - 49:5(2013), pp. 2116-2125. [10.1109/TIA.2013.2258876]

Availability:
This version is available at: 11583/2507496 since:

Publisher:
IEEE

Published
DOI:10.1109/TIA.2013.2258876

Terms of use:

This article is made available under terms and conditions as specified in the corresponding bibliographic description in the repository

Publisher copyright

(Article begins on next page)

30 October 2026

Experimental Identification of the Magnetic Model of Synchronous Machines

E. Armando, R. Bojoi, P. Guglielmi, G. Pellegrino and M. Pastorelli
Dipartimento Energia - Politecnico di Torino
Corso Duca degli Abruzzi, 24 - Torino, 10129 ITALY

***Abstract*—The paper proposes and formalizes a comprehensive experimental approach for the identification of the magnetic model of synchronous electrical machines of all kinds. The identification procedure is based on controlling the current of the machine under test while this is driven at constant speed by another, regenerative electric drive. Compensation of stator resistance and inverter voltage drops, iron loss, operating temperature issues are all taken into account. A road map for implementation is given, on different types of hardware setups. Experimental results are presented, referring to two test motors of small size, and references of larger motors identified with the same technique are given from the literature.**

I. Introduction

Over the last years, the research work regarding the electrical synchronous machines and their control has focused on the machine design optimization and also on optimal control techniques able to fully exploit the machines characteristics. That was induced and supported by a continuous penetration of synchronous machines in many industrial applications, as well as in traction and automotive applications, home appliances and power generation for renewable systems. The most employed synchronous machine solutions include Surface Mounted Permanent Magnet (SPM) machines, Synchronous Reluctance (SyR) machines and Interior Permanent Magnet (IPM) machines. All mentioned machines need accurate modeling of their magnetic model, both for design and control purposes.

The magnetic model is the relationship between the machine currents and the machine flux linkages in a specific reference frame. As known from the literature, the most convenient reference frame that should be used for the magnetic model identification is the rotor synchronous (d, q) frame [1]–[9]. Even with the proper axes choice, the magnetic model representation and experimental identification are non trivial efforts, especially for those machines exhibiting significant magnetic saturation and cross-saturation. As a general assumption, the (d, q) machine flux linkages are a non linear function of both $d-$ and $q-$axis current components.

The synchronous machines that are renowned for being highly non-linear due to saturation and cross-saturation are the IPM and the SyR ones [1]–[7]. However, the same problem has been reported for saturated (i.e. compact and overloaded) SPM machines [8], [9].

The benefits of the experimental identification of the magnetic model of such machines are:

1) the motor performance (torque, power versus speed profile with limited voltage and current) can be off-line calculated with precision.
2) In particular, the determination of the Maximum Torque per Ampere (MTPA) and the Maximum Torque per Volt (MTPV) control trajectories is mandatory for the full exploitation of the motor torque and speed ranges.
3) The performance comparison of motors provided by different manufacturers is made possible, without the need of insights about design, materials and manufacturing.

The latter point can be important for choosing between different motor suppliers. It results that the magnetic model is crucial for a proper machine evaluation and also for an optimal control strategy, including sensorless operation [10], [11].

The literature reports several methods for magnetic model identification, divided into *analytical/simulation methods* and *methods based on experimental measurements*. The first methods are usually based on Finite Element Analysis (FEA) [6] and/or analytical computations [7] based on equivalent magnetic circuits. These methods can be used only by the machine designers since they need all information regarding the motor design. The experimental methods are useful when only machine rated data are available.

The experimental methods can be divided into *standstill methods* and *constant-speed methods*. The standstill methods are well known for wound-field synchronous machines [12], [13], without taking into account the saturation and cross-saturation. A locked rotor method that takes into account all saturation effects is presented in [1], where voltage pulses are applied to one axis (e.g. d), while a constant current is controlled along the other axis (e.g. q). This method is very effective, but requires integration of the applied voltage, that is critical and prone to drift due to offsets. Moreover, the voltage level to be handled by the inverter during the tests is very low and then potentially imprecise, in particular for motors with a low per-unit resistance. Stator resistance variations are compensated, but no clue is given about the PMs temperature and what the effect of core loss on the magnetic curves is. In [2], the flux-linkages are evaluated at constant speed via the measurement of the $d-$ and $q-$axis voltages when a couple of constant (d, q) current components is impressed to the machine. The voltage is measured at the machine terminals and then low-pass filtered for pulse-width modulation (PWM) harmonics elimination. A compensation of the filter attenuation and phase is necessary, as well as a FFT

scheme for fundamental components extraction. The solution presented in [2] does not take into account the stator resistance variation during the test. This may be a problem when the magnetic model is evaluated in overload current conditions. The stator resistance variation can be mitigated by increasing the test speed, but this may increase the iron losses, that are not taken into account, either.

This paper proposes a comprehensive experimental approach for the identification of the magnetic model of any synchronous electrical machine. The machine is running at steady-state speed and current, and the flux linkages are obtained from the evaluation of the (d, q) voltage components, as in [2]. The stator resistance variation is compensated here, allowing the magnetic model identification for any current level. Three voltage estimation methods are compared, showing that easier-to-implement rigs can give reasonable accuracy, without the need for analog measurement of the PWM voltages. Voltage harmonics due to spatial harmonics and inverter dead-time effects are averaged during the signal acquisition without complicate post-processing, such as FFT. Iron loss are taken into account, and it is suggested how to avoid them to interfere with the identification process. The operating temperature is monitored, since temperature variations would distort the magnetic curves of PM-based machines.

The identification methodologies have been applied to two motors of small size: one SyR machine one IPM machine of the PM-assisted SyR (PMASR) type.

II. Measurement Procedure

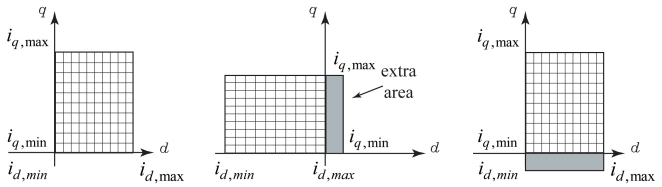
The goal of the identification procedure is to evaluate the steady-state machine flux linkages, in dq coordinates, synchronous to the rotor, as a function of the corresponding current components (1):

$$\begin{cases} \lambda_d = f\left(i_d, i_q\right) \\ \lambda_q = f'\left(i_d, i_q\right) \end{cases} \tag{1}$$

The area of evaluation of the model is a rectangle, in the dq current plane, delimited within the ranges $i_{d,min}$ to $i_{d,max}$ and $i_{q,min}$ to $i_{q,max}$, that must include all the operating conditions of interest for the drive under test, i.e. continuous and transient overload points. The risk of demagnetization must be also taken into account for machines with PMs. The current area is organized in a regularly spaced grid, defined by the equally spaced arrays of current values (2):

$$\begin{cases} i_{d,k} = i_{d,min} + k \cdot \Delta i_d & k = 1, 2, 3.. \\ i_{q,k'} = i_{q,min} + k' \cdot \Delta i_q & k' = 1, 2, 3.. \end{cases} \tag{2}$$

In Fig. 1 three examples of current grid are given for different motor and reference axes types: SyR motors are identified for positive values of i_d and i_q and the model in all other quadrants follows for symmetry (Fig. 1a). PM machines are identified for positive i_q values and negative, flux-weakening, i_d, as in Fig. 1b, both for IPM and SPM motor types. The PMASR machine resembles a SyR rather than a IPM and then SyR axes are still adopted, as in Fig. 1b. For all machines with PMs it is convenient to extend the identification area into the flux-intensifying region, colored in gray in Fig. 1 b and c, for including transient working points either in flux-controlled drives or drives adopting a flux-observer [14], [15].



(a) SyR (b) IPM, SPM (c) PMASR

Fig. 1. dq current mesh.

For the sake of flux linkage identification, the steady-state voltage equation of the synchronous machine is considered (3), e.g. with reference one of the points of the identification grid $(i_{d,k}, i_{q,k'})$:

$$\begin{cases} v_{d,kk'} = R_s \cdot i_{d,k} - \omega_e \cdot \lambda_{q,kk'} \\ v_{q,kk'} = R_s \cdot i_{q,k'} + \omega_e \cdot \lambda_{d,kk'} \end{cases} \tag{3}$$

where ω_e the electrical speed and R_s is the stator resistance. From (3), the flux linkages can be evaluated as:

$$\begin{cases} \lambda_{d,kk'} = \frac{v_{q,kk'} - R_s \cdot i_{q,k'}}{\omega_e} \\ \lambda_{q,kk'} = -\left(\frac{v_{d,kk'} - R_s \cdot i_{d,k}}{\omega_e}\right) \end{cases} \tag{4}$$

For reproducing the steady state conditions properly, the experimental setup is organized as follows:

- the machine under test is driven at constant speed by a speed controlled servo motor (constant ω_e) and the speed is measured;
- the machine under test is vector current controlled at $(i_{d,k}, i_{q,k'})$;
- the PWM voltages are measured or accurately estimated;
- the stator resistance voltage drop must be compensated;
- in case of PM machines, all tests must be at the same operating temperature;
- the effect of iron loss must be negligible.

In the following, all those aspect are analyzed in detail.

A. Current control sequence for series voltage drop compensation

As said, the (i_d, i_q) region under analysis includes transient overload conditions. In other words, all tested points at overload current may produce rapid variations of the operating stator and magnets temperature even in short times. To keep temperature variations under control, the active test time at each set of currents $(i_{d,k}, i_{q,k'})$ should be as short as possible. On the other hand, current pulses should last as long as needed to guarantee that the unavoidable speed regulation transient is extinguished and that all measures (voltages, currents, speed) are *logged at least over one mechanical period, and then averaged*, to eliminate any signal component at electrical or mechanical periodicity, including motor space harmonics, inverter dead-time harmonics and defects of mechanical nature such as misalignments and eccentricities.

To compensate for the voltage drop on the stator resistance in (4), the voltage vector is first measured in motoring mode,

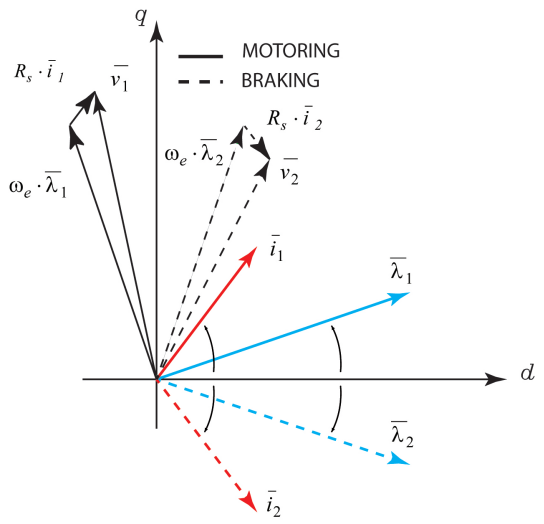


Fig. 2. Steady-state vector diagrams (current, flux linkage and voltage) of a Synchronous Reluctance machine in motoring (subscript 1) and braking (subscript 2) conditions: current vectors 1 and 2 are complex conjugates and also the respective flux linkage vectors are.

e.g. with the current vector being $(i_{d,k} + j \cdot i_{q,k'})$. Straight away, the complex conjugate current vector $(i_{d,k} - j \cdot i_{q,k'})$ is imposed, referring to braking conditions, and the voltage vector is again measured. From (4), the average between the voltage vectors in motoring and braking turns out to be independent of the resistive term. In Fig. 2 it is shown, for an example SyR machine, that the two complex conjugate current vectors 1 and 2 produce complex conjugates flux linkage vectors, and the respective voltage vectors differ only in the sign of the resistive drop. All other series voltage drops, such as inverter on-state and dead-time voltage errors, are compensated by the average between motoring and braking modes, at least for what concerns their fundamental component. As said above, sixth and multiple harmonics of the inverter error are inherently compensated by averaging all the variables over one mechanical period.

Besides the two conjugate current pulses needed to average motoring and braking, a third and final test pulse is included, again in motoring, to eliminate any possible resistance variation during the first two pulses, as represented in Fig. 3. In case the temperature varies during the current pulses, the average temperature of the two motoring tests (first and third pulses) will be equal to the average temperature of the braking test (pulse number two), and so it will be the stator resistance value, as shown in Fig. 3. In most of practical implementations, the duration of the current pulses is much shorter than the thermal time constant of the motor, and the resistance variation between the first and the third pulse is negligible. Experimental evidence is given at section IV for one of the example machines under test.

All considered, the flux estimation from the three-pulse test is obtained composing (4) over the three pulses, according to the vector diagram of Fig. 2, under the assumption of constant speed:

$$\lambda_d = \frac{1}{2} \cdot \left(\frac{v_{q,1} + v_{q,3}}{2} + v_{q,2} \right) \cdot \frac{1}{\omega_e} \tag{5}$$

$$\lambda_q = -\frac{1}{2} \cdot \left(\frac{v_{d,1} + v_{d,3}}{2} - v_{d,2} \right) \cdot \frac{1}{\omega_e} \tag{6}$$

The subscripts $1, 2$ and 3 stand for the three pulses from which one point of the flux linkage map is evaluated. The electrical speed in (5) is logged in the same time window of the voltage and current measures, and must be the same for the three pulses, indicated in Fig. 3. As said, the time window for data logging must be equal to one mechanical turn, as also represented in the figure.

It must be remarked here that exploiting the machine under test both in motoring and braking implies that *both the drives, the one supplying the machine under test and the speed controlled servo motor drive must be regenerative or have an adequate braking chopper*. The power size of the braking chopper is not a critical issue, for either drives. In fact, the instantaneous regenerated power is under the rated power of the machine under test, because the test speed is half or less than half the rated one, as addressed at subsection II-C. Moreover, the regeneration mode has a limited duty-cycle, corresponding to the duration of one or two of the three current pulses out of the period of one current sequence, including idle mode. One pulse refers to the machine under test, that is twice motoring and once braking per cycle, and vice-versa for the speed-controlled prime mover (see Fig. 4).

B. Motor temperature and thermal conditioning

Once the duration of the three current pulses is determined and minimized as long as possible, the idle time between one test working point and the next one, represented in Fig. 4, can be chosen in a way that the motor temperature remains stable, that is of particular importance when dealing with permanent magnet machines. Theoretically, it is always possible to choose the idle time point by point for keeping the average temperature of the machine constant during the whole identification, given the duration of the three current pulses. This however can complicate the implementation of

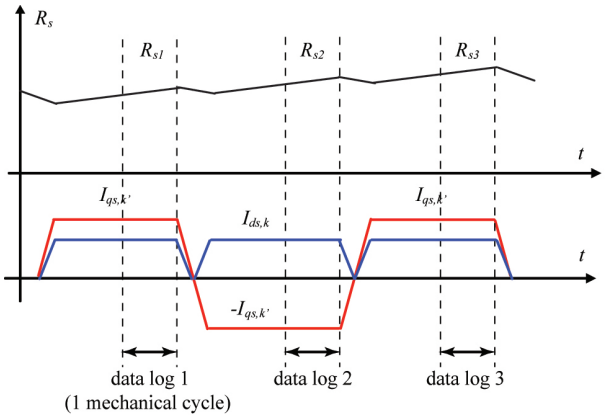


Fig. 3. R_s variation due to temperature during the three-pulses evaluation of point $(i_{d,k}, i_{q,k'})$: the average of R_{s1} and R_{s3} equals R_{s2}.

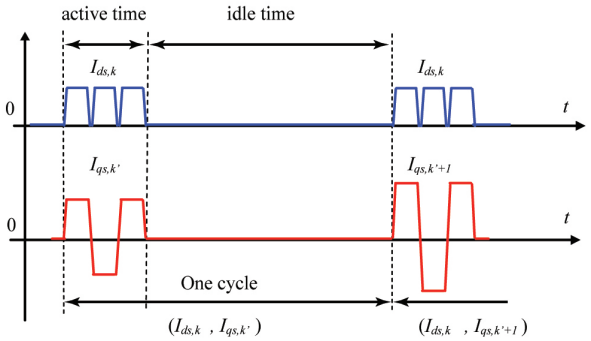


Fig. 4. Example of i_d and i_q pulse sequence with "idle time" twice the "active time", as adopted in the reported experimental tests.

the identification algorithm and can also lead to unpractical overall identification times in some cases, in particular if the duration of the current pulses is not correctly minimized.

In case of a PM machine, it is convenient to warm it up to the required thermal conditions and then monitor the temperature during the whole identification process. The PM temperature monitoring can be made automatic by measuring the motor voltage during the idle state intervals, when the machine current is controlled to zero current and the motor voltage coincide with the PM-flux generated back-emf.

For all the machines under test the measurements have been done with the idle time being twice the active time and monitoring the end windings temperature.

C. Iron loss effect and correct speed level

A robust control of the constant speed and the choice of the speed level are both key issues.

Dealing with the latter point, the speed should be as high as to produce significant levels of v_d and v_q, with a good signal to noise ratio for voltage measurement. From this point of view the speed should be placed around the rated motor speed, that is also the rated voltage condition. Moreover, the speed has to be as low as needed for having a negligible contribution of the speed dependent loss, that is iron loss and, if the case, PM loss. Fig. 5 shows how the two vector diagrams in motoring and braking of Fig. 2 are no longer symmetrical once iron loss is not negligible: the controlled current vectors are complex conjugates ($\bar{i}_2 = \bar{i}_1^*$, where the subscript $*$ indicates the complex conjugate), but the flux linkage vectors are not ($\bar{\lambda}_2 \neq \bar{\lambda}_1^*$): in fact, the non negligible core loss current vectors $\bar{i}_{Fe}$ result in two magnetizing current vectors that are different in amplitude and no longer specular in phase: $\bar{i}_2' \neq (\bar{i}_1')^*$. Vector diagrams for a PM based machine would have different angles but would still lead to the same conclusions.

A good tradeoff speed is normally one third of the base speed.

D. Voltage measurement

Voltage measurement is another critical issue. The most accurate but difficult to tune solution is based on analog measurement of the motor terminal voltages, then analog rotational transformation, analog filtering of the PWM components

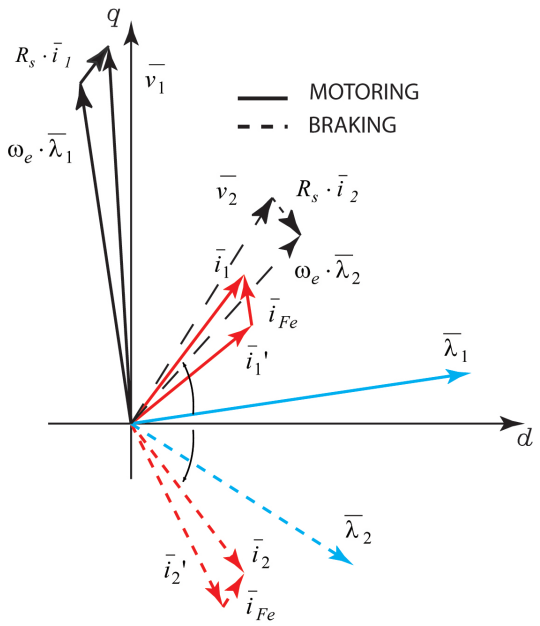


Fig. 5. Steady-state vector diagrams of a SyR machine in motoring (1) and braking (2) conditions with complex conjugates current vectors: the flux linkages are no longer complex conjugate due to iron loss.

and then analog to digital conversion of the obtained dq components. A cheaper solution reconstructs the voltages from the inverter duty-cycle commands and the DC-link voltage measurement: a proper inverter dead-time compensation is mandatory in this case. An intermediate solution can be to measure the duty-cycles of the three phase voltages by means of three voltage comparators and a time capture unit, as shown in section III).

TABLE I
OUTLINE OF THE PROPOSED IDENTIFICATION STRATEGY

Prime mover	Speed controlled drive with 4 quadrant operation chopper
Front end supply	Regenerative or braking chopper
Braking chopper rating	<< motor continuous power
Torque meter	Not needed
Measurement of motor voltages	Not strictly needed
Copper temperature variations	Compensated, ref. (5),(6)
PM temperature	Can be stabilized by proper timing (ref. II-B)
Core loss	Negligible, according to speed choice (ref. II-C)

III. Hardware Implementation

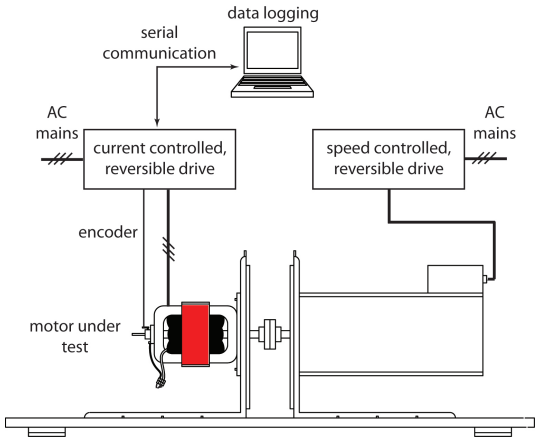
The identification procedure has been implemented on different hardware setups. In general, two test rig schemes are possible:

1) the machine under test is coupled to a speed-controlled, reversible servo drive, as in Fig. 6(a). The torque rating of the servo drive must be redundant with respect to

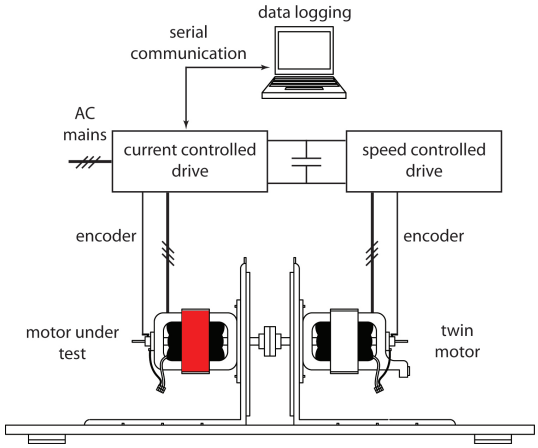
the maximum transient overload torque of the machine under test.

2) the drive under test (machine plus inverter) is duplicated, the two inverters are back to back connected to a common dc-link, and the two machines are directly coupled, as in Fig. 6(b). One drive is speed controlled, the other is current controlled.

The adoption of one technique or the other one depends on the available facilities, but it can be said that the former scheme is more suitable for small to medium size machines, once a suitable regenerative servo-drive has been set up. The latter solution is normally adopted for large prototype machines, exceeding the torque size of the servo drive based rig. Such dual scheme is somehow preferable because it avoids the need for braking resistors or reversible AC/DC stages. However, if the two machines are actually identical, the inspected overload current area should be likely slightly restricted according to the actual capability of the speed controlled machine to keep the speed constant during the tests. In other words: if the two machines are actually identical there is no torque redundancy, that would be still welcome.



(a) regenerative servo rig



(b) back to back rig

Fig. 6. Scheme of the two test bench adopted in the machine characterization

A. Adopted rigs

Three experimental setups have been used for producing the results presented in section IV. Converters A and B refer to the "regenerative servo rig" scheme of Fig. 6(a) and are associated to a servo-drive of appropriate size. Two converters of type C are back to back connected as in Fig. 6(b). Most of all, the three solutions differ for the voltage measurement or reconstruction method they adopt.

- Converter A (Fig. 7(a)) has analog voltage measures.
- Converter B (Fig. 7(b)) reconstructs the voltages by means the control reference duty-cycles and the measured dc-link voltage, with dead-time correction.
- In converter C (Fig. 7(c)) the voltages are reconstructed by time capturing the duty-cycles and multiplying by the measured dc-link voltage.

More in detail, converter A has Hall-effect current sensors with scale adjustable from 10Apk to 200Apk and 600V dc-link. Current measurements and current control are managed by an on-board floating-point DSP. The mechanical position is measured according to which transducer is available on the motor under test: where not specified, the standard transducer in the tests is a 512 pulses incremental encoder. Line voltages are measured by means of operational amplifiers in differential configuration. Then, the dq voltage components are calculated by analog multiplication with sine and cosine of the electrical rotor angle given by the DSP via digital-to-analog conversion. The so obtained $\hat{V}_{dq}$ are sampled by two precision multimeters synchronized with the sampling instant always by the motor-control DSP.

Converter B is for small motors, being based on a commercial DMC1500 power board, by Spectrum Digital Inc., controlled by a dSPACE 1103 micro controller board via a prototype interface board. Current measures are again from Hall-effect sensors, rated 9Apk max. Voltage measurements are available, but with this converter the (d, q) voltages are estimated by means of the control reference voltages v^*_{dq}, with dead-time correction [16].

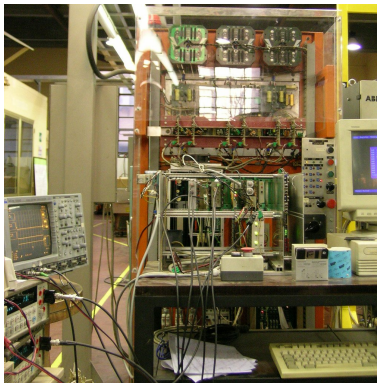
Converter C is a prototype converter based on IRAM10B06A intelligent power modules, purposely built to control small motors for appliances with two different current sensors: Hall-effect and shunt resistors. The on board fixed-point MCU (micro controller unit) is a Freescale MC56F8323. Phase voltages are captured by the MCU for measuring the actual duty-cycles: from the duty-cycles and the dc-link voltage measure it is possible to estimate the phase voltages quite accurately, apart from the on-state voltage drops of the power switches. Commands and communications are performed via an insulated CAN (Controller Area Network) bus, while all measurement are performed inside the MCU and sent to an external PC via the communication line.

B. Motors under test

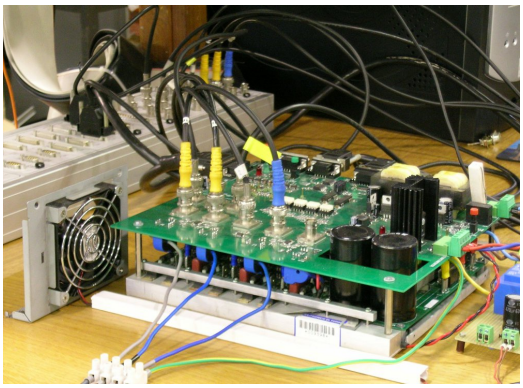
The motors under test are:

- a SyR motor;
- a PM-Assisted SyR motor (PMASR).

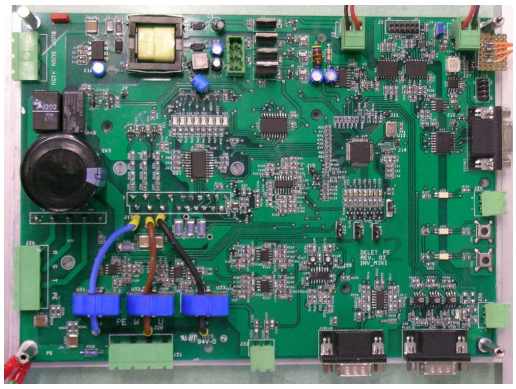
In fact, those are two prototype motors with the same laminations, represented in Fig. 8, having the rotors without



(a) Converter A



(b) Converter B



(c) Converter C

Fig. 7. Power converters adopted for the identification procedure: A) with analog voltage measurement equipment; B) dSPACE based inverter, with voltage estimation from the control reference voltages; C) inverter with fixed-point DSP and time capture of the phase voltage duty-cycles.

magnets (sub-figure a) and with the magnets assembled (sub-figure b), respectively. Due to the SyR nature of both the motors, the reference axes from now on are according to the SyR style. In particular, this means that the PM flux linkage, if the case, is aligned to the negative q axis (Fig. 9(b)).

The ratings of the PMARS motor are: 1 Nm nominal torque, 2.8 Apk nominal current, 200 V, base speed 3000 rpm, maximum operating speed 15000 rpm. The SyR version can reach 8000 rpm at no load due to the lower power factor. Flux linkage versus current maps have been investigated in a square area in the dq current plane delimited by $0 < i_q < 5A$ and $0 < i_d < 5A$. The reference dq axes are chosen according

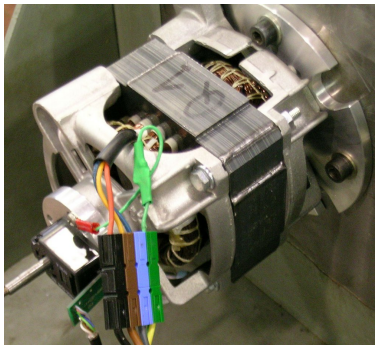


Fig. 8. Prototype motor for home appliances: test machine 1 refers to a SyR rotor and test machine 2 to a PM-assisted SyR rotor, reported in Fig. 9, assembled into identical stators.

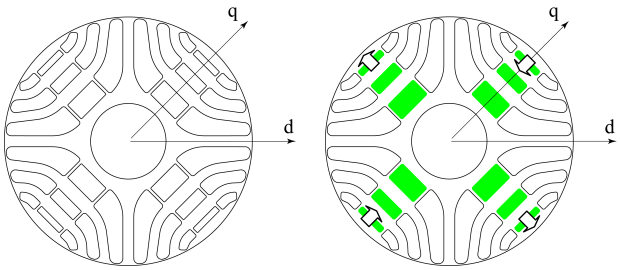


Fig. 9. Sketch of the rotor laminations of the two test motors: a) SyR; b) PMASR.

to the SyR convention, for the sake of an easier comparisons between the two motors.

The same identification technique has been applied in the past to larger machines, both of the SyR and IPM types, up to 250 kW for SyR [17] and up to 1 MW for IPM [18].

C. Current pulse signs with different d-axis conventions

The sequencing of current pulse signs is of key importance for obtaining symmetric motor and generator operations as the ones reported in the vector diagram of Fig. 2, representative of a SyR machine. The q current component is reversed in this case, an the current sequence has the form reported in Fig. 4. When dealing with PM machines, the possibility of two different d-axis conventions can create some confusion, and lead to an erroneous implementation.

With the most common convention of having the d axis aligned with the PM flux linkage, the inversion of the q current component and the waveforms of Fig. 4 are still correct. However, PMASR machine drives are often associated to the SyR axes convention, as indicated in Fig. 9(b) for the test motor of this paper. In this latter case it is the d current that must be reversed, and not the q component, as will be also shown in the following section. In general, it is the *current component in quadrature with the PM flux linkage* the correct one to be conjugated.

IV. Experimental Results

Both the example machines have been identified with all the three hardware setups, and the results are similar in the three cases for each machine.

As a first example, the flux linkage curves identified with converter A (analog voltage measures) and the ones obtained with converter B (estimation from control reference voltages) are reported in Fig. 10(a) for the SyR motor. For clarity of comparison, only the extreme curves of the flux linkage maps are plotted: the ones with no cross current component (e.g. λ_d with $i_q = 0$) and the ones with the maximum cross-current value (e.g. λ_d with $i_q = 5$ A). It can be noticed that the two sets of curves are very similar, in particular when the cross current component is zero. The curves with cross-current - $\lambda_d(i_d, 5\text{ A})$ and $\lambda_q(i_d, 5\text{ A})$ - show little differences that have no practical consequences. The differences between the flux linkage curves obtained with the two rigs are reported in Fig. 10(b), showing to be very limited over the entire current range.

In Fig. 11 the flux linkage curves of the PMASR motor are reported: this time the ones identified with converter A (analog voltage measures) are compared with the ones obtained with the two converters of type C, back to back connected, and with the voltage estimation based on the duty-cycle measurement. Again, the two sets of curves are very similar. The difference between the dashed and the continuous curves here is more evident and somehow unavoidable, with respect to Fig. 10. In fact, the voltage estimate from the duty-cycle measurement has a systematic error due to on-state voltage drop, that are not compensated in this case. On the other hand, voltage estimate from reference duty cycles (dashed lines in Fig. 10) gives results that are closer to the ones with analog measures.

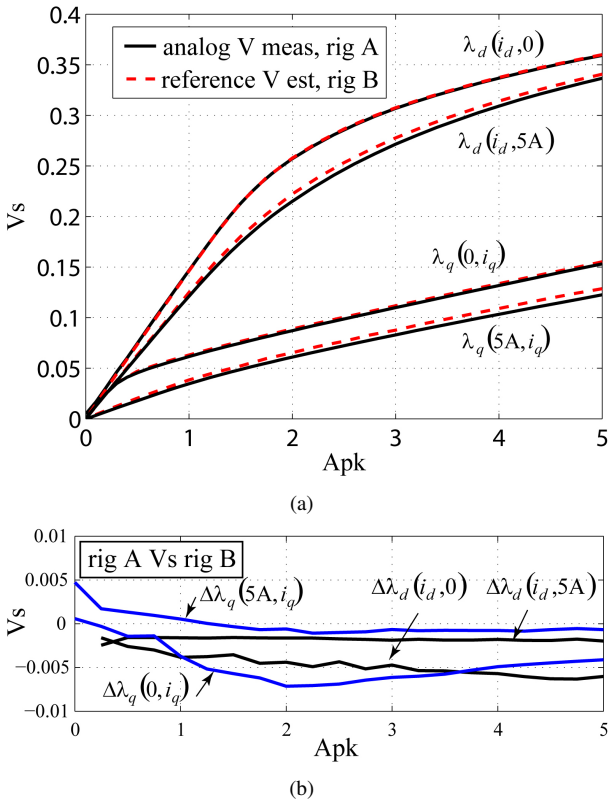


Fig. 10. a) (d, q) flux linkages versus current components for the SyR test motor. Analog voltage measures (rig A) and voltage estimation from control reference voltages (rig B) are compared. b) Flux estimation error, evaluated as the difference between the rig A curves minus the respective rig B curves.

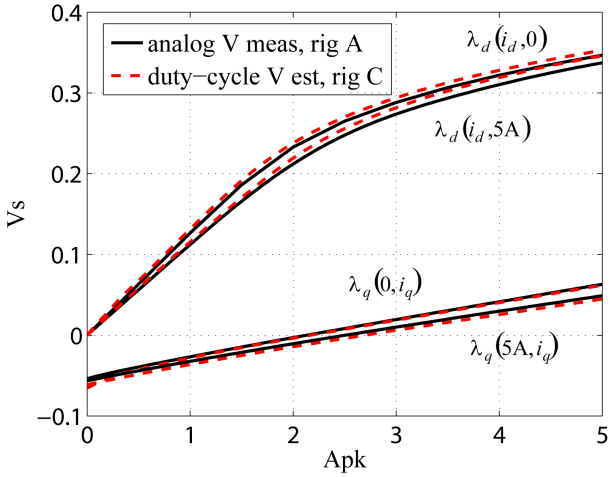


Fig. 11. (d, q) flux linkages versus current components for the PM-assisted SyR test motor. Analog voltage measures (rig A) and voltage estimation from duty-cycle measurement (rig C) are compared.

In Fig. 12 the dq current and voltage waveforms referring to current points $\bar{i}_{dq} = 2 + j0$ A and $\bar{i}_{dq} = 2 + j4$ A are reported, for the PM-assisted machine and rig A. As said, it is the i_d component here to be reversed when dealing with braking conditions, instead of the i_q one as done in Fig. 4 for the SyR machine.

In Fig. 13, the voltage waveforms are represented in detail, in proximity of one of the data log time windows of test point $\bar{i}_{dq} = 2 + j4$ A. Voltage measurements are compared to the voltage reference signals of the current controllers. The latter are overestimated, due to the lack of inverter non linearities compensation on this test rig, where control voltages where not meant to be used for voltage estimation and motor identification. The time window corresponds to one mechanical turn, to filter off all periodic disturbances possibly affecting the v_d and v_q signals. In Fig. 13 there is an evident second harmonic term superimposed to both the measured and estimated voltage signals. This harmonic term is probably due to the response of the dq current regulators to non perfectly compensated current offsets.

A. Motor performance evaluation

Once the flux linkage surfaces are identified in the (d, q) current plane, the steady state performance of the test machines can be comprehensively evaluated through the basic machine equations. Torque is calculated over the (d, q) current identification area via (7):

$$T = \frac{3}{2} \cdot p \cdot (\lambda_d \cdot i_q - \lambda_q \cdot i_d) \tag{7}$$

The current vector is given, the flux vector is known, the voltage vector can be calculated, in amplitude and phase, from the voltage equation (3). All such variables (current, flux linkage, voltage, torque) are then represented by surfaces in the (d, q) plane, whose contour lines can be also easily evaluated : as an example, constant torque curves are reported in Fig. 14, along with the 5 A current circle. The fundamental control trajectories can be then evaluated: for example, the MTPA and MTPV reported in Fig. 14 are obtained by intersection of

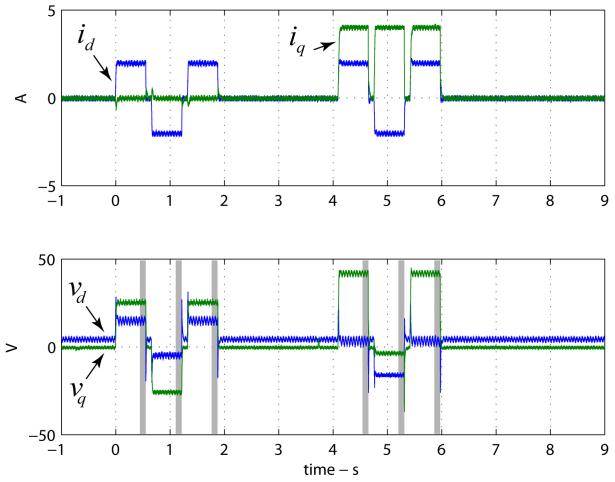


Fig. 12. Example of dq current and analog measured voltage waveforms during the identification of the PM-assisted SyR with rig A, at 600 rpm. The tested working points are: $i_{dq} = 2 + j0$ A and $i_{dq} = 2 + j4$ A. Gray boxes indicate data log windows.

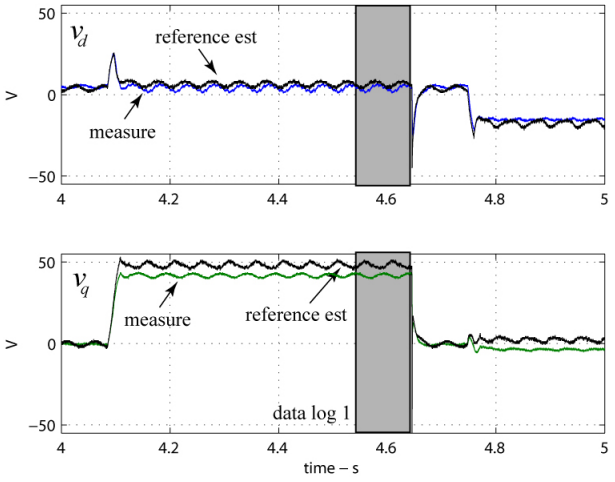


Fig. 13. Detail of Fig. 12 in a time window between 4 and 5 s, containing the comparison between analog measured voltages and current control reference voltages.

constant-current and constant-flux contours with the constant-torque contours, respectively.

Once the control trajectories are known, the motor performance can be forecast: the torque and torque per Ampere characteristics are reported in Fig. 15, referring to MTPA operation. The curves are reported for the two cases of analog voltage measures (continuous line) and voltage estimation from the control reference voltages (dashed), showing negligible differences. The power versus speed profile at limited inverter voltage is also calculated, as reported in Fig. 16, where MTPA operation is assumed below base speed, then constant voltage constant current operation and, finally, MTPV operation [19].

B. Application to vector current control

In vector current control of synchronous motors, the magnetic model is utilized for building control look-up tables, mainly for the exploitation of the MTPA trajectory and also,

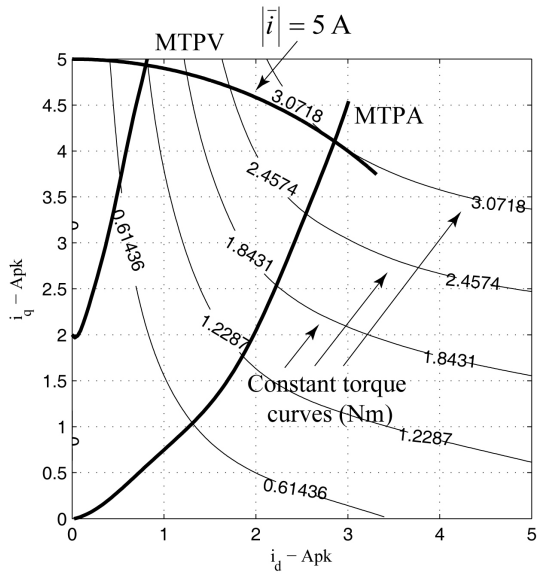


Fig. 14. Test PMASR motor: constant torque curves, maximum peak current curve and MTPA and MTPV trajectories calculated according to the experimental magnetic model.

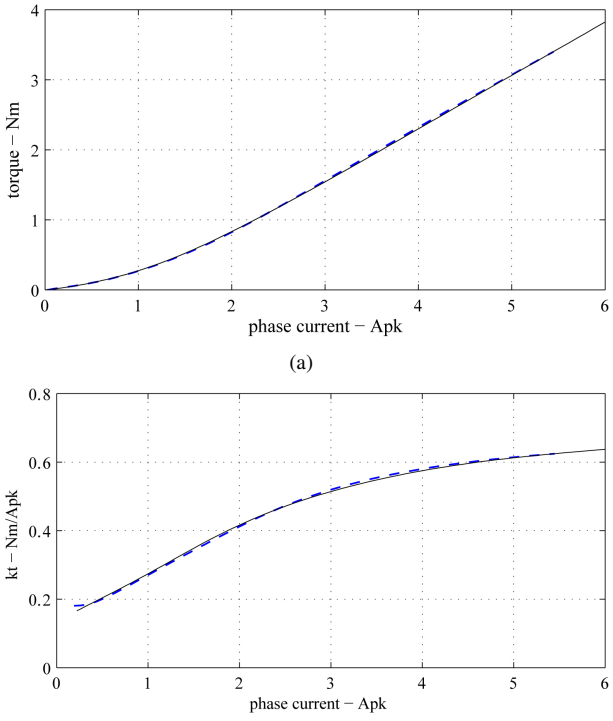


Fig. 15. Test PMASR motor, torque performance along the MTPA control trajectory. a) Torque versus phase peak current; b) Nm/A versus phase peak current. The black, continuous lines refer to analog voltage measures (rig A) and the dashed blue lines refer to control reference voltages (rig B).

for flux-weakening [20]. As an example of a current control scheme with a light use of the motor model, the control scheme of [20] is reported in Fig. 17, while many other schemes require even heavier manipulations of the motor model to fill more look-up tables [21]. The d and q MTPA current references of the PMASR test motor are reported in Fig. IV-B:

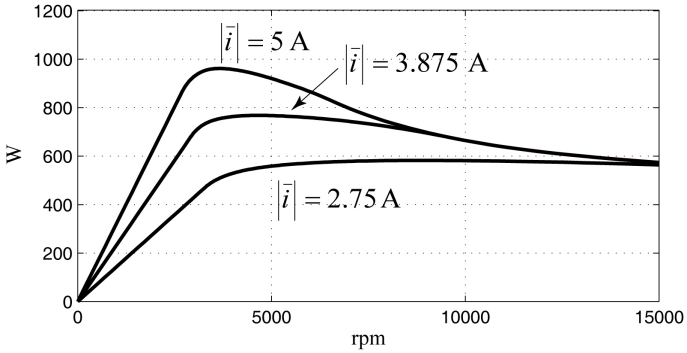


Fig. 16. Test PMASR motor: output power versus curves at 270 V DC-link voltage and different peak current levels.

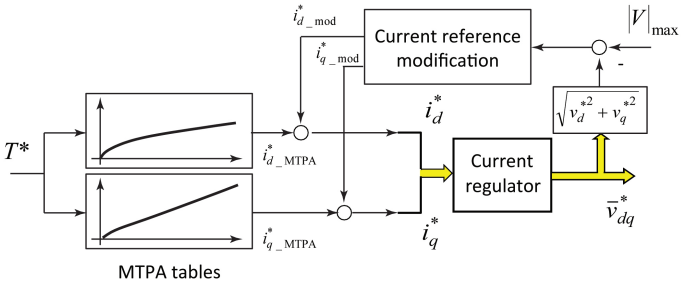


Fig. 17. Example of vector current control scheme [20]. The "MTPA tables" and the "Current reference modification" blocks come from the manipulation of the motor magnetic model.

they have been calculated by manipulation of the experimental flux-linkage curves of Fig. 11.

C. Application to Direct-Flux and Direct-Torque control

Direct-flux and direct torque controls are less model dependent than current vector control, dealing in particular with flux-weakening mode. However, for high efficiency at low loads, it is convenient to adjust the flux amplitude reference of a SyR or an IPM motor according to the torque reference, following the MPTA control law. As an example, the control scheme of [14] is represented in Fig. 19, showing the look-up table for flux amplitude regulation. The torque to flux amplitude reference table is also reported in Fig. 20, for the test PMASR motor, again obtained by manipulation of the experimental flux-linkage curves of Fig. 11.

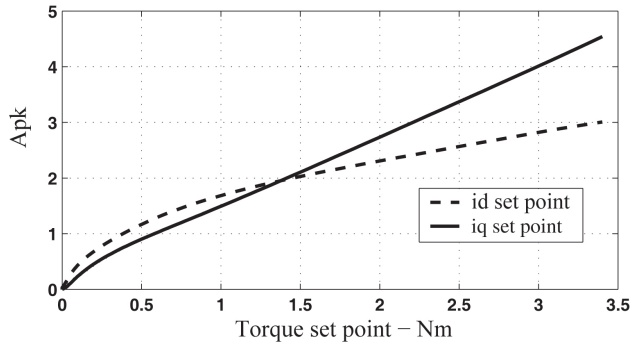


Fig. 18. Test PMASR motor: current reference tables for MTPA operation with current vector control.

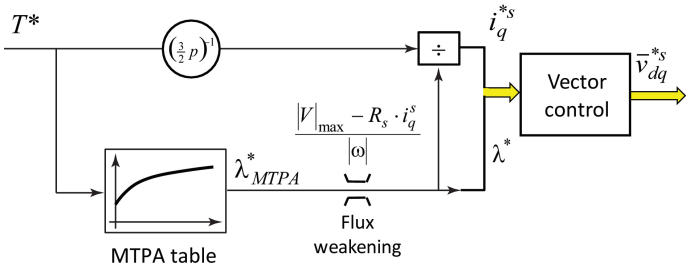


Fig. 19. Example of direct flux, field oriented vector control scheme [14]. The MTPA flux reference table block comes from the manipulation of the motor magnetic model.

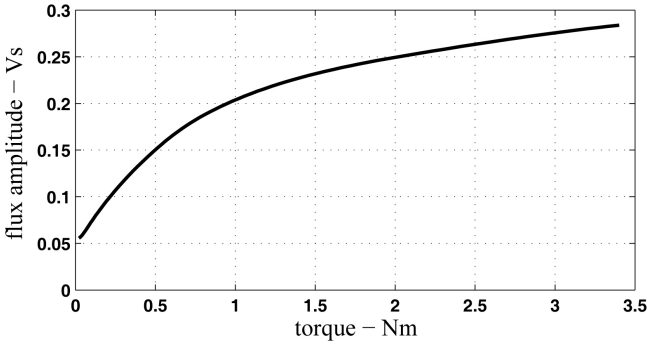


Fig. 20. Test PMASR motor: flux amplitude reference table for MTPA operation with direct-flux vector control.

V. Conclusion

This paper formalizes a procedure for the experimental identification of the magnetic model of synchronous electrical machines. The machine flux linkages are represented as a function of the machine stator currents in the rotor synchronous reference frame. Once the magnetic model is identified, the motor control trajectories can be calculated and the motor performance can be defined in detail. The magnetic model can be used:

- to evaluate a new machine design of for comparing existing designs, especially for machines with highly non linear magnetic behavior;
- it is mandatory for control implementation in those applications with critical aspects, such as deep flux weakening speed range, position sensorless control at zero and low speed or optimized efficiency at all loads.

Three different hardware setups have been compared, with different techniques for the measurement or estimation of the PWM motor voltages and different layouts of the respective test rigs. Two test motors have been considered, one SyR and one PM-Assisted SyR, and examples of identification of larges motors have been referenced. The analysis formalizes the identification procedure and demonstrates that this is consistent also when performed with a standard inverter, with no special hardware features such as accurate analog voltage measures.

References

[1] B. Stumberger, G. Stumberger, D. Dolinar, A. Hamler, and M. Trlep, "Evaluation of saturation and cross-magnetization effects in interior

permanent-magnet synchronous motor," *Industry Applications, IEEE Transactions on*, vol. 39, no. 5, pp. 1264 – 1271, sept.-oct. 2003.

[2] K. Rahman and S. Hiti, "Identification of machine parameters of a synchronous motor," *Industry Applications, IEEE Transactions on*, vol. 41, no. 2, pp. 557 – 565, march-april 2005.

[3] R. Dutta and M. Rahman, "A comparative analysis of two test methods of measuring - and -axes inductances of interior permanent-magnet machine," *Magnetics, IEEE Transactions on*, vol. 42, no. 11, pp. 3712 –3718, nov. 2006.

[4] P. Guglielmi, M. Pastorelli, and A. Vagati, "Impact of cross-saturation in sensorless control of transverse-laminated synchronous reluctance motors," *Industrial Electronics, IEEE Transactions on*, vol. 53, no. 2, pp. 429 – 439, april 2006.

[5] E. Armando, P. Guglielmi, G. Pellegrino, M. Pastorelli, and A. Vagati, "Accurate modeling and performance analysis of ipm-pmasr motors," *IEEE Trans. on Industry Applicat.*, vol. 45, no. 1, pp. 123 –130, 2009.

[6] N. Bianchi and S. Bolognani, "Magnetic models of saturated interior permanent magnet motors based on finite element analysis," in *IEEE Industry Applications Conference IAS 1998*, vol. 1, Oct. 1998, pp. 27 –34 vol.1.

[7] K. Meessen, P. Thelin, J. Soulard, and E. Lomonova, "Inductance calculations of permanent-magnet synchronous machines including flux change and self- and cross-saturations," *Magnetics, IEEE Transactions on*, vol. 44, no. 10, pp. 2324 –2331, oct. 2008.

[8] A. Wijenayake and P. Schmidt, "Modeling and analysis of permanent magnet synchronous motor by taking saturation and core loss into account," in *IEEE Conference on Power Electronics and Drive Systems PEDS 1997*, vol. 2, May 1997, pp. 530 –534 vol.2.

[9] T. Frenzke, "Impacts of cross-saturation on sensorless control of surface permanent magnet synchronous motors," in *European Conference on Power Electronics and Application EPE 2005*, 0 2005.

[10] R. Morales-Caporal and M. Pacas, "Impact of the magnetic cross-saturation in a sensorless direct torque controlled synchronous reluctance machine based on test voltage signal injections," in *IEEE Conference on Industrial Electronics IECON 2008*, 2008, pp. 1234 –1239.

[11] D. Reigosa, P. Garcia, D. Raca, F. Briz, and R. Lorenz, "Measurement and adaptive decoupling of cross-saturation effects and secondary saliencies in sensorless controlled ipm synchronous machines," *IEEE Trans.on Industry Applicat.*, vol. 44, no. 6, pp. 1758 –1767, 2008.

[12] L. Le and W. Wilson, "Synchronous machine parameter identification: a time domain approach," *Energy Conversion, IEEE Transactions on*, vol. 3, no. 2, pp. 241 –248, jun 1988.

[13] E. Boje, J. Balda, R. Harley, and R. Beck, "Time-domain identification of synchronous machine parameters from simple standstill tests," *Energy Conversion, IEEE Transactions on*, vol. 5, no. 1, pp. 164 –175, mar 1990.

[14] G. Pellegrino, E. Armando, and P. Guglielmi, "Direct-flux vector control of ipm motor drives in the maximum torque per voltage speed range," *Industrial Electronics, IEEE Transactions on*, vol. 59, no. 10, pp. 3780 –3788, oct. 2012.

[15] A. Yoo and S.-K. Sul, "Design of flux observer robust to interior permanent-magnet synchronous motor flux variation," *Industry Applications, IEEE Transactions on*, vol. 45, no. 5, pp. 1670 –1677, sept.-oct. 2009.

[16] G. Pellegrino, R. Bojoi, P. Guglielmi, and F. Cupertino, "Accurate inverter error compensation and related self-commissioning scheme in sensorless induction motor drives," *Industry Applications, IEEE Transactions on*, vol. 46, no. 5, pp. 1970 –1978, sept.-oct. 2010.

[17] G. Pellegrino, E. Armando, P. Guglielmi, and A. Vagati, "A 250kw transverse-laminated synchronous reluctance motor," in *Power Electronics and Applications, 2009. EPE '09. 13th European Conference on*, sept. 2009, pp. 1 –10.

[18] G. Pellegrino, A. Vagati, and P. Guglielmi, "Design tradeoffs between constant power speed range, uncontrolled generator operation, and rated current of ipm motor drives," *Industry Applications, IEEE Transactions on*, vol. 47, no. 5, pp. 1995 –2003, sept.-oct. 2011.

[19] S. Morimoto, Y. Takeda, T. Hirasa, and K. Taniguchi, "Expansion of operating limits for permanent magnet motor by current vector control considering inverter capacity," *Industry Applications, IEEE Transactions on*, vol. 26, no. 5, pp. 866 –871, sep/oct 1990.

[20] Y.-D. Yoon, W.-J. Lee, and S.-K. Sul, "New flux weakening control for high saliency interior permanent magnet synchronous machine without any tables," in *Power Electronics and Applications, 2007 European Conference on*, sept. 2007, pp. 1 –7.

[21] B.-H. Bae, N. Patel, S. Schulz, and S.-K. Sul, "New field weakening technique for high saliency interior permanent magnet motor," in *Industry Applications Conference, 2003. 38th IAS Annual Meeting. Conference Record of the*, vol. 2, Oct. 2003, pp. 898–905 vol.2.